Molecular BioSystems

PAPER

View Article Online
View Journal

Cite this: DOI: 10.1039/c6mb00304d

Histidine switch controlling pH-dependent protein folding and DNA binding in a transcription factor at the core of synthetic network devices†

D. K. Deochand, I. C. Perera,‡ R. B. Crochet,§ N. C. Gilbert, M. E. Newcomer and A. Grove*

Received 20th April 2016,
Accepted 7th June 2016

DOI: 10.1039/c6mb00304d

www.rsc.org/molecularbiosystems

Therapeutic strategies have been reported that depend on synthetic network devices in which a urate-sensing transcriptional regulator detects pathological levels of urate and triggers production or release of urate oxidase. The transcription factor involved, HucR, is a member of the multiple antibiotic resistance (MarR) protein family. We show that protonation of stacked histidine residues at the pivot point of long helices that form the scaffold of the dimer interface leads to reversible formation of a molten globule state and significantly attenuated DNA binding at physiological temperatures. We also show that binding of urate to symmetrical sites in each protein lobe is communicated *via* the dimer interface. This is the first demonstration of regulation of a MarR family transcription factor by pH-dependent interconversion between a molten globule and a compact folded state. Our data further suggest that HucR may be utilized in synthetic devices that depend on detection of pH changes.

Introduction

Metabolic pathways are highly integrated, and dysregulation can lead to an array of metabolic disorders. The conventional approach to treatment involves administration of small molecule drugs, but this approach may lead to undesirable side effects due to off-target activities. To combat this problem, synthetic circuits have been developed in which pathological concentrations of a specific metabolite are sensed; this event in turn triggers a corrective response designed to restore cellular homeostasis.[1–3]

On this basis, urate-responsive network devices have been created that can sense pathological concentrations of urate. One such device consists of a transcription factor that mediates dose-dependent derepression of a gene encoding urate oxidase upon sensing elevated levels of urate.[4] A second device that takes advantage of the same transcription factor consists of a hydrogel in which interaction between the transcription factor and its cognate DNA crosslinks the hydrogel to trap urate oxidase; upon sensing urate, dissolution of the hydrogel results in release of urate oxidase and degradation of excess urate.[5] Urate is the final product of purine degradation in humans and excess can lead to diseases such as gout or tumor lysis syndrome.[6,7] These diseases involve excess urate in the bloodstream or deposition of uric acid crystals in joints, kidneys, and other tissues; in many patients, hyper-uricemia is due to increased purine salvage as a result of faster cellular turnover caused by proliferative or inflammatory disorders or from tissue hypoxia.[8] Thus, maintaining urate homeostasis in the body is essential.

Both reported urate-sensing devices were constructed by exploiting the properties of *Deinococcus radiodurans* HucR (hypothetical uricase regulator), which belongs to the multiple antibiotic resistance regulator (MarR) family of transcription factors.[9] MarR family transcriptional regulators are ubiquitous and modulate key cellular functions in bacteria and archaeae, such as metabolic pathways, virulence, stress responses, neutralization of reactive oxygen species, and degradation and export of antibiotics or other harmful chemicals.[10–13] Most MarR family proteins bind cognate DNA with high affinity and specificity, and most are repressors and prevent gene expression by sterically hindering the binding of RNA polymerase to the promoter. Repressor binding is often attenuated in

Department of Biological Sciences, Louisiana State University, Baton Rouge, LA 70803, USA. E-mail: agrove@lsu.edu

† Electronic supplementary information (ESI) available: Figures showing gel filtration chromatography of all proteins at pH 5.0, EMSA of HucR-H51F at room temperature and pH 5.0; EMSA of all proteins at 4 °C and pH 5.0, thermal denaturation of all proteins in complex with DNA at pH 8.0 and 5.0, HucR structure illustrating ligand-binding site, intrinsic tryptophan fluorescence of all proteins in presence of ligands urate and xanthine, and schematic of conformational changes in HucR. Tables showing secondary structure content estimated from CD spectra, T_m of all proteins in absence and presence of urate, data collection and refinement statistics for crystal structure of HucR-E48Q, and procedures for preparation of HucR mutant proteins. See DOI: 10.1039/c6mb00304d

‡ Present address: Department of Zoology, University of Colombo, Sri Lanka.
§ Present address: Case Western Reserve University, Cleveland, OH, USA.

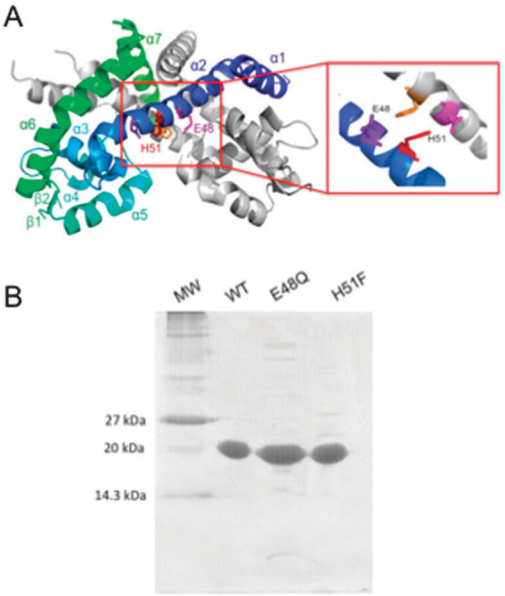

Fig. 1 HucR variants. (A) Stacked H51/H51′ at the dimer interface of HucR-WT. Cartoon representation of HucR-WT with one monomer colored blue to green (N- to C-terminus) and the other monomer in gray. The close-up view shows H51/H51′ in red and orange and neighboring E48/E48′ in magenta. (B) Purified HucR-WT, HucR-E48Q, and HucR-H51F in 15% SDS-PAGE gel. Molecular weight (M_w) markers are shown at the left.

presence of small molecule ligands, leading to derepression of gene expression.[12–17]

In *D. radiodurans*, HucR represses expression of a gene encoding urate oxidase by binding a cognate site in the gene promoter with high affinity.[9] In the presence of the ligand urate, the repression is relieved. These properties make HucR an ideal sensor of urate in synthetic gene network devices. The crystal structure of HucR revealed that it is a dimer with two DNA binding lobes that are spatially configured to interact with consecutive DNA major grooves.[18] The framework of the dimerization region is provided by long intersecting helices, one from each subunit. At the pivot point of these helices, two histidine residues are stacked, a configuration that raises the possibility that the dimer interface is sensitive to changes in pH (Fig. 1A).

We report here that stacked histidine residues at the dimer interface of HucR act as a reversible pH sensor, responsible for a pH-dependent interconversion between a molten globule and a compact folded state. Our data also indicate that DNA and ligand binding is communicated through the dimer interface. Considering the highly conserved fold of MarR family transcriptional regulators, communication through the dimer interface may be a shared characteristic of this essential class of transcription factors in which ligand- and DNA-binding are not confined to separate domains. Our observations suggest that HucR binding to DNA is not only sensitive to urate, but also to pH, and they suggest possibilities for engineering pH-sensitivity into closely related proteins. Thus, this system could be used to design more generic sensors or synthetic devices applicable to diseases that involve metabolic acidosis, such as diabetes, osteoporosis, cardiovascular damage, or ulcer by integrating different metabolites in functional biomaterials.[19,20]

Results and discussion

Structure of HucR predicts pH sensitive function

HucR was previously shown to exist as a dimer in which each monomer contributes a dimerization region and a DNA binding lobe with overall topology α1–α2–α3–β1–α4–α5–β2–β3–α6–α7 (Fig. 1A).[18] The DNA binding region is composed of α3–β1–α4–α5–β2–β3, which adopts the winged-helix fold that is characteristic of MarR family proteins. In unliganded HucR, the two DNA binding lobes are positioned such that the distance between recognition helices (α5) match the distance between consecutive DNA major grooves. Members of the MarR protein family are obligate dimers; in HucR, the dimerization domain is formed by helices α2, α6, and α7, and the dimer interface is maintained by intersecting α2 and α2′ from each monomer. The two monomers are extensively intertwined, as reflected in a buried surface area of ~6300 Å^2. At the pivot point of the long α2 helices, the imidazole rings of H51 and H51′ are stacked and separated by 3.6 Å. At pH 7.0 (the pH at which the crystals were obtained) and above, the imidazole rings of histidine would be expected to be largely deprotonated, permitting stable stacking interactions[21] whereas protonation would be predicted to result in charge repulsion;[22] positive charges would be stabilized by interaction with neighboring E48/E48′. Since the protonation state of the imidazole group (pK_a ~ 6.5) is likely to be significantly pH dependent under physiological conditions as well as dependent on the local environment, we speculated that H51 could serve as a pH sensor, wherein protonation of His residues causes conformational change in the protein due to charge repulsion and E48 serves to raise the pK_a of imidazole rings to ensure pH sensitivity within a physiologically relevant range. To assess the effect of pH on HucR function, we created two mutants, HucR-H51F (to abolish pH effect; Phe was chosen because the shape of the side chain is similar to a neutral His and paired Phe residues likewise prefer a stacked conformation)[23] and HucR-E48Q (to remove charge stabilization, which is expected to increase the pK_a of His51 in HucR-WT compared to HucR-E48Q). Both HucR mutants were overexpressed in *E. coli* and purified to apparent homogeneity (Fig. 1B).

Histidine protonation disrupts the protein fold

To assess the effect of pH on the HucR variants, we determined thermal stability of the proteins at pH 8.0, pH 7.0, pH 6.0, and pH 5.0 using differential scanning fluorometry. SYPRO Orange was used as fluorescent reporter, as it binds nonspecifically to hydrophobic patches when protein unfolds as a function of temperature.[24] The thermal stability of HucR-WT, HucR-E48Q, and HucR-H51F were similar at pH 8.0 and pH 7.0 with melting temperatures (T_m) of ~52 °C (Fig. 2 and Table 1). By comparison, the T_m of HucR-WT was previously determined by circular dichroism spectroscopy, revealing a two-state melting transition with T_m ~ 51 °C in phosphate buffer at pH 7.0.[9] Thus, despite the slightly higher temperature coefficient for HEPES

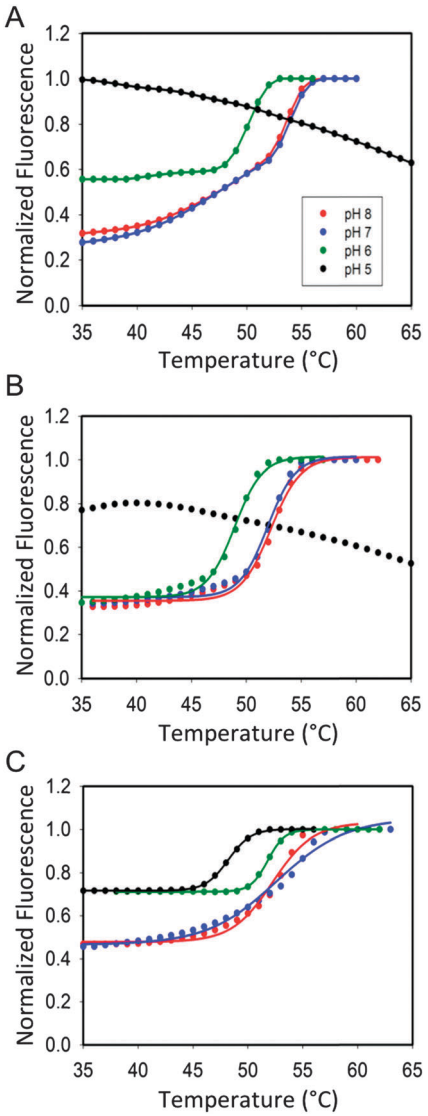

Fig. 2 Thermal stability determined by fluorometry. Normalized fluorescence of SYPRO Orange bound to hydrophobic patches of unfolded protein/molten globule states as a function of temperature at pH 8.0 (red), 7.0 (blue), 6.0 (green), and 5.0 (black). (A) HucR-WT. (B) HucR-E48Q. (C) HucR-H51F.

($-0.014\Delta pK_a/°C$; resulting in a pH $\sim$ 6.6 at the T_m) compared to phosphate ($-0.0028\Delta pK_a/°C$) and the use of SYPRO Orange as a reporter of unfolding, the T_m obtained for HucR-WT is consistent. The higher temperature coefficient for Tris ($-0.031\Delta pK_a/°C$) would result in a pH $\sim$ 7.1 at the T_m. Both HucR-WT and HucR-E48Q were modestly destabilized at pH 6.0 with a decrease in T_m of $\sim$2 °C, whereas HucR-H51F remained stable ($T_m \sim 52$ °C; for MES, the temperature coefficient of $-0.011\Delta pK_a/°C$ would result in a pH $\sim$ 5.7 at the T_m).

At pH 5.0, HucR-WT and HucR-E48Q were severely destabilized and no melting curves were observed (the negligible temperature coefficient of $-0.0002\Delta pK_a/°C$ for acetate would not be expected to result in significant pH changes with temperature). Moreover, the magnitude of initial fluorescence was very high, suggesting that the proteins were in an unfolded or molten globule state at the start of the temperature scan (5 °C). SYPRO Orange shares with 1-anilino-naphtalene-8-sulfonate (ANS), which is commonly used to detect the presence of molten globule states, a higher affinity for hydrophobic patches exposed either due to complete unfolding or formation of molten globule intermediates.[25] This observation supports the interpretation that both HucR-WT and HucR-E48Q were destabilized due to protonation of H51/H51′ at pH 5.0. Notably, the observed destabilization was fully reversible upon deprotonation; for both HucR-WT and HucR-E48Q, raising the pH of proteins previously equilibrated at pH 5.0 to pH 8.0 restored a two-state melting curve with a $T_m \sim 52$ °C (Table 1). By contrast, thermal unfolding of HucR-WT was previously found to be irreversible.[9]

These observations suggest that the stacked histidine residues at the dimer interface function as a molecular switch, effecting a pH-dependent interconversion between a molten globule and a compact folded state.

In contrast, HucR-H51F remained stable at pH 5.0, and an unfolding transition was observed with $T_m \sim 48$ °C. We therefore infer that protonation of H51/H51′ was a primary contributor to the observed destabilization of HucR-WT and HucR-E48Q. The observed modest destabilization of HucR-H51F may be associated with protonation of other histidines. Since marginal destabilization of HucR-H51F was detectable at pH 5.0 whereas HucR-WT and HucR-E48Q were severely destabilized, we infer that the pK_a of H51 (regardless of the presence of E48) is higher than that of other residues associated with destabilization at pH 5.0. Submission of the structures of HucR-WT (2FBK) and HucR-E48Q (see below) to the DEPTH server[26] for prediction of pK_a values revealed a predicted pK_a for H51 of $\sim$5.5 for HucR-WT and $\sim$5.2 for HucR-E48Q, consistent with the expected decrease in pK_a for HucR-E48Q and with significant destabilization of both proteins at pH 5.0. By comparison, the surface-exposed H25 and H142 have predicted pK_a values near 6.5 and H147 has a $pK_a \sim 4.2$ in both proteins, suggesting that protonation of H147 may contribute to protein destabilization at pH 5.0. Since HucR-H51F is only marginally destabilized at pH 5.0, however, we infer that the contribution of H147

Table 1 Melting temperature (T_m) as a function of pH and in presence of DNA (°C)

Protein	pH 5.0	pH 6.0	pH 7.0	pH 8.0	pH 5.0/8.0[a]	+DNA (pH 8.0)	+DNA (pH 5.0)
HucR-WT	n/a	49.9 ± 0.1	51.4 ± 0.5	51.6 ± 0.4	52.2 ± 0.3	51.8 ± 0.2	21.8 ± 0.1
HucR-E48Q	n/a	48.9 ± 0.1	51.9 ± 0.1	52.2 ± 0.1	52.8 ± 0.4	52.2 ± 0.1	26.8 ± 0.1
HucR-H51F	48.2 ± 0.0	51.8 ± 0.0	52.3 ± 0.2	52.7 ± 0.1	nd	52.3 ± 0.1	40.2 ± 0.4

[a] T_m of protein initially equilibrated at pH 5.0, followed by equilibration at pH 8.0. nd, not determined. All T_m values determined based on SYPRO Orange fluorescence.

protonation to the observed changes in protein stability is modest. Considering the very marginal destabilization of HucR-WT observed at pH 6.0 (Table 1) we also infer that protonation of surface-exposed H25 and H142 is unlikely to affect protein stability.

To address the inference that a molten globule state was induced at pH 5.0, circular dichroism spectroscopy was performed. A molten globule would be characterized by maintained or increased secondary structure content.[27,28] As shown in Fig. 3A, CD spectra of all three proteins were characterized by significant secondary structure content at pH 7.0, with α-helical content of 55–64% (calculated based on mean residue molar ellipticity; ESI,† Table S1); for HucR-E48Q (which was estimated to have the lowest α-helical content), we speculate that the greater magnitude of the ellipticity may be due to less contributions of aromatic residues to the far UV CD signal.[29] A change in the magnitude of the ellipticity for HucR-E48Q suggests that the mutation caused changes in structure or dynamics of the protein.

At pH 5.0, all proteins retained secondary structure content ((Fig. 3B); 62–67% α-helix; Table S1, ESI†); the ellipticity for HucR-WT was markedly decreased at pH 5.0 compared to pH 7.0. Measurement of thermal stability at pH 5.0 for HucR-H51F showed a cooperative unfolding transition with $T_m \sim 53$ °C (Fig. 3D). We ascribe the difference in T_m determined by CD spectroscopy and SYPRO Orange fluorescence to changes in tertiary structure associated with exposure of hydrophobic patches that may be detected by SYPRO Orange binding, but not by CD, which reflects changes in secondary structure content only. In contrast, a very gradual, non-cooperative increase in ellipticity was observed for both HucR-WT and HucR-E48Q (Fig. 3C). These observations support the interpretation that HucR-WT and HucR-E48Q were in a molten globule state at pH 5.0 whereas HucR-H51F was in a native folded state.

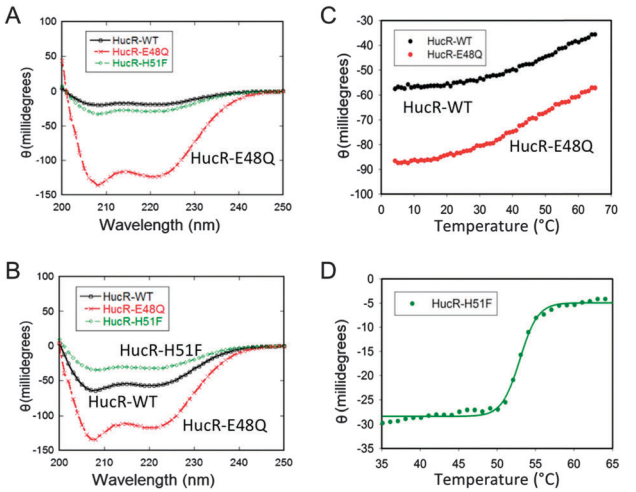

Fig. 3 CD spectral analysis of HucR variants. (A) CD spectra of HucR-WT (black), HucR-E48Q (red), and HucR-H51F (green) at pH 8.0. (B) CD spectra of HucR-WT (black), HucR-E48Q (red), and HucR-H51F (green) at pH 5.0. (C and D) Thermal stability of HucR variants at pH 5.0. Ellipticity was recorded at 218–224 nm in CD2 buffer (50 mM sodium phosphate pH 7.0 or 50 mM acetate pH 5.0, both with 100 mM NaCl). (C) HucR-WT (black) and HucR-E48Q (red). (D) HucR-H51F.

The equilibrium sedimentation profile of HucR in absence of DNA was previously shown to reflect a single non-associating species with a molecular mass corresponding to a dimer at pH 8.0.[30] This indicates that measurements of protein stability are uncomplicated by monomer-dimer equilibria at this pH. To assess the oligomeric state of HucR variants at pH 5.0, gel filtration chromatography was performed. The oligomeric state of HucR-WT was verified at pH 7.0, where the protein eluted as a single species with $M_w \sim 43$ kDa, corresponding to a dimer (ESI,† Fig. S1A and B). Similar elution profiles were observed for all three protein variants at pH 5.0, except that a minor species that eluted with $M_w \sim 6$ kDa was observed for HucR-WT and HucR-E48Q (Fig. S1C–E, ESI†). This indicates that all proteins remain largely dimeric at pH 5.0, and that the reduced protein stability at pH 5.0 is not due to a significant presence of monomeric species.

Histidine protonation results in attenuated DNA binding at physiological temperatures

To investigate the effect of pH on DNA binding by HucR proteins, electrophoretic mobility shift assays (EMSA) were performed at pH 8.0 and pH 5.0. For HucR-WT, it was previously shown that the apparent K_d is unaltered on reducing pH from 8.0 to 6.0.[18] A 77 bp DNA containing a single HucR-binding site was used (Fig. S2, ESI†). At pH 8.0, HucR-WT and HucR-E48Q formed complex with an apparent dissociation constant (K_d) of 1.0 ± 0.1 and 1.4 ± 0.1 nM, respectively, indicating high affinity binding (Fig. 4). However, HucR-H51F bound DNA with lower affinity (K_d = 13.6 ± 1.8 nM). Notably, while HucR-WT and HucR-H51F formed a single complex, HucR-E48Q formed multiple complexes; consistent with this observation, titration with non-specific DNA revealed that DNA binding specificity was lost in the E48Q mutant whereas HucR-H51F retained sequence-specific binding (data not shown). The different mode of DNA binding by HucR-E48Q is consistent with the inference from CD spectroscopy that the mutation resulted in altered structure or dynamics of the protein. Taken together, these observations indicate that modulation of the dimer interface affects DNA binding, as reflected in reduced DNA binding affinity by HucR-H51F and loss of specificity by HucR-E48Q. That changes in the dimerization region affect DNA binding has been previously reported for other MarR homologs.[31,32] This communication between dimerization and DNA-binding regions likely depends on α2 helices, whose C-terminal halves contact the helix-turn-helix motif (Fig. 1A).

Attempts at measuring binding affinity at pH 5.0 revealed significant instability of protein–DNA complexes when DNA binding assays were performed at room temperature with HucR-WT and HucR-E48Q (data not shown), suggesting that histidine protonation compromised DNA binding. In contrast, stable complex was still detectable with HucR-H51F (Fig. S2, ESI†). This is consistent with HucR-H51F adopting a native folded conformation at pH 5.0, whereas both HucR-WT and HucR-E48Q existed in a molten globule state. That complexes with HucR-WT and HucR-E48Q were unstable also suggests that DNA-binding did not restore formation of the native folded state in these proteins.

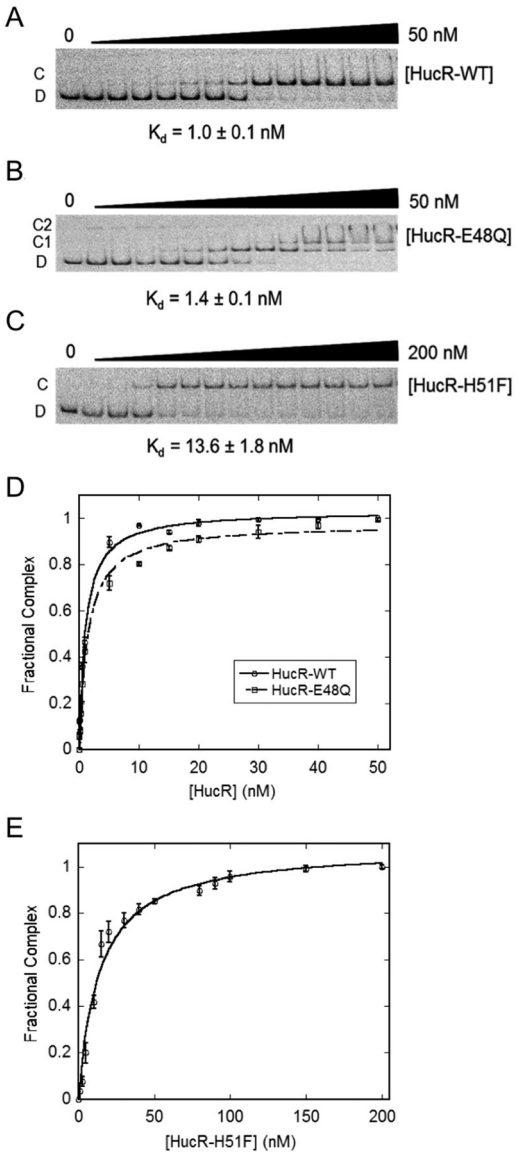

Fig. 4 DNA binding affinity at pH 8.0. (A–C) Electrophoretic mobility shift assay of HucR-WT, HucR-E48Q, and HucR-H51F binding to 0.1 nM *hucO* (77-bp) at room temperature. The sequence of the HucR binding site is shown in Fig. S2 (red) (ESI†). Complex (C) and free DNA (D) are indicated at the left. (D) Binding isotherms for HucR-WT (continuous line) and HucR-E48Q (broken line). (E) Binding isotherm for HucR-H51F. Error bars represent standard deviation from three independent experiments.

When DNA binding assays were instead performed at 4 °C, stable protein–DNA complexes were detected (Fig. S3A–C, ESI†). At pH 5.0, DNA binding affinity of HucR-WT (K_d = 13.7 ± 5.7 nM) was significantly reduced, as reflected in an ~14-fold increase in K_d compared to pH 8.0 (measured at room temperature; Fig. S3A, D, F, ESI†). This is consistent with the interpretation that protonation of stacked histidine residues at the dimer interface leads to conformational changes that propagate to the DNA binding lobes. In contrast, HucR-E48Q bound DNA with an only modest decrease in DNA binding affinity (K_d = 2.6 ± 0.9 nM) (Fig. S3B, D, F, ESI†). Removal of E48 prevents the formation of a salt bridge with protonated H51 and would be expected to lower the pK_a of H51; the reduced pH sensitivity of HucR-E48Q would be consistent with this expectation. In addition, it is possible that the absence of H51-E48 interactions confers flexibility to the dimer interface that permits conformational changes associated with DNA binding to occur with less penalty. It is also conceivable that such increased flexibility, which suggests the existence of a population of alternative conformations, enables the protein to bind more divergent sequences, as reflected in the observed loss of sequence specificity. HucR-WT and HucR-H51F bind a single site, and the apparent K_d reflects the affinity for this site. In contrast, HucR-E48Q has reduced sequence specificity and forms multiple complexes; accordingly, the apparent K_d should be considered a macroscopic binding constant, and the microscopic K_d reflecting affinity for a single site would be higher. We also note that the calculated K_d underestimates the decrease in binding affinity of protonated protein since a population of unprotonated protein is likely to exist; indeed, the possibility exists that complex formation is due to the population of protein that remains unprotonated. HucR-H51F also had reduced DNA binding affinity at pH 5.0 (K_d = 63.6 ± 8.8 nM), however, binding affinity was decreased by only ~5-fold (Fig. S3C, E, F, ESI†). These data show that HucR-H51F is less sensitive to pH compared to HucR-WT. That HucR-H51F exhibited pH-sensitivity may be due to protonation of additional His residues of which one (H25) is located immediately following α1, in the loop connecting α1 and α2, and two are in α6, H142 on the protein surface and H147 facing the ligand-binding pocket that bridges the DNA-binding lobes and the dimer interface.[18,32]

HucR-WT and HucR-E48Q were in a molten globule state at pH 5.0, yet protein–DNA complex was observed at 4 °C; therefore, we reasoned that DNA stabilized the proteins at pH 5.0. We performed the thermal stability assay of all three proteins in complex with 40 bp DNA containing the cognate site at pH 5.0 and 8.0. At pH 5.0, HucR-WT and HucR-E48Q were stabilized on DNA binding (T_m of 21.9 and 26.8 °C, respectively; Fig. S4, ESI† and Table 1), with DNA binding most efficiently restoring a closely packed conformation of HucR-WT as evidenced by reduced initial fluorescence. However, DNA binding evidently did not fully restore the native folded state observed at pH 8.0, and the T_m of protein–DNA complexes is consistent with the observed instability of complexes during electrophoresis at room temperature. In contrast, HucR-H51F was destabilized in presence of DNA at pH 5.0, with a decrease in T_m of ~8 °C. At pH 8.0, the thermal stability of all three proteins in complex with DNA was similar to that of proteins with no DNA, with T_m ~ 52 (Fig. S4A, ESI† and Table 1).

Contacts to the DNA are expected to be stabilizing (and yield a higher T_m) assuming preferred binding to native folded protein. However, protein is flexible and will sample the ensemble of conformational states, and this model does not account for DNA preferentially binding to (and stabilizing) the unfolded state or a subpopulation of protein whose thermal stability is lower than the ensemble average.[33] At pH 5.0, HucR-WT and HucR-E48Q exist in a molten globule state that appears to be converted to a native folded state on DNA binding, resulting in a cooperative unfolding transition. However, the low T_m implies that complex

formation will not occur at a physiological temperature of 37 °C. At pH 8.0, the observation that DNA binding does not result in an increase in thermal stability suggests that DNA preferentially binds a less-stable subpopulation, stabilizing this state, in the process resulting in a shift in the population upon binding towards the conformer with highest affinity for ligand.[34] Similarly, DNA complexes with HucR-H51F at pH 5.0 are less stable than the unbound protein, suggesting preferred DNA binding to a less-stable subpopulation.

Ligand-binding is communicated across the dimer interface

To examine whether modification of the dimer interface also had an effect on ligand binding, we measured intrinsic tryptophan fluorescence of HucR-WT and mutant proteins as a function of ligand concentration. We used urate and xanthine (Fig. S5, ESI†), as these molecules attenuate HucR–DNA complex formation.[9,16,30] Both compounds are intermediates in the purine degradation pathway. As reported previously, HucR has two ligand-binding sites in which four conserved residues (W20, D73, R80, and R106) are predicted to interact with urate or connect the ligand-binding site to the DNA-binding lobes (Fig. S5, ESI†).[16] Analysis of fluorescence quenching confirmed the previous observation that urate bound HucR-WT with K_d = 11.4 ± 2.9 μM and Hill coefficient n_H = 0.7 ± 0.1, indicating negative cooperativity. Urate bound HucR-E48Q with higher affinity (K_d = 2.2 ± 0.8 μM), retaining negative cooperativity. In contrast, HucR-H51F bound urate with K_d = 14.7 ± 1.2 μM, and positive cooperativity was observed with n_H = 2.1 ± 0.2 (Fig. S6, ESI†). Xanthine showed similar binding affinity (K_d ~ 17 μM) for all three proteins, and positive cooperativity (n_H ~ 2) was consistently observed. The change from negative to positive cooperativity on binding of urate and xanthine was previously reported for HucR-WT.[16] Docking of urate in the ligand-binding pocket predicts a hydrogen bond between urate N7 and the carbonyl oxygen of M41 in α2, directly connecting bound ligand to the dimer interface. However, while unfavorable interactions between urate O12 and the carbonyl oxygen of L44 of α2 are predicted, xanthine lacks O12, perhaps leading to the observed differences in cooperativity. That urate binding to HucR-H51F likewise showed positive cooperativity of binding may reflect a conformational change that alleviates such unfavorable contacts to urate. The exact basis for the noted differences in cooperativity notwithstanding, these observations indicate that the dimer interface is involved in communicating occupancy of one ligand-binding site to the other.

Further, we performed thermal shift assays to determine the effect of urate on stability of proteins at pH 8.0 (the limited solubility of urate precludes analysis at pH 5.0). Addition of 10 μM urate to HucR-WT resulted in a two-step melting transition, as measured by SYPRO Orange fluorescence, with T_m ~ 41 °C for step one and T_m ~ 52 °C for step two (Fig. 5A and Table S2, ESI†). When measured by CD spectroscopy, however, a single cooperative transition was observed with T_m = 53.0 ± 0.1 °C (Fig. 5E), corresponding to a modest decrease in thermal stability compared to unliganded protein (T_m = 54.4 ± 0.1 °C; Fig. 5D). Considering the K_d for urate of ~11 μM, two populations

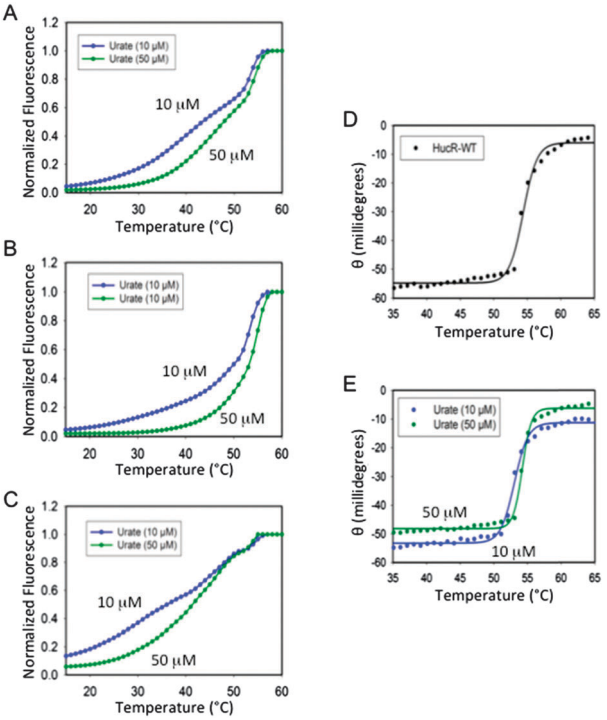

Fig. 5 Thermal denaturation of HucR variants incubated with urate at pH 8.0. (A–C) Thermal denaturation measured by normalized SYPRO Orange fluorescence. (A) HucR-WT. (B) HucR-E48Q. (C) HucR-H51F. (D and E) Thermal stability of HucR-WT measured by CD spectroscopy at 218–224 nm. (D) HucR-WT supplemented with 0.1 M NaOH (the solvent for urate). (E) HucR-WT with 10 μM urate (blue) or 50 μM urate (green).

should be present; one corresponding to urate-bound protein and one corresponding to protein with no ligand bound. Given the negative cooperativity of urate binding, we also infer that the urate-bound population is likely to reflect predominantly protein in which only one ligand-site is occupied. Since both methods indicated that urate resulted in a modest destabilization at a concentration at which HucR likely consists largely as a mixture of unbound and singly liganded protein, we surmise that initial unfolding of urate-bound HucR may primarily change tertiary structure and result in exposure of hydrophobic patches, resulting in increased SYPRO Orange fluorescence, whereas overall changes in secondary structure content are minor. We also infer that occupancy of a single site destabilizes HucR. At higher concentration of urate (50–100 μM), the probability of both ligand-binding sites being occupied is higher, and a shift of the melting transition towards higher temperatures is evident by both methods (Fig. 5A, E and Table S2, ESI†). While the K_d for urate binding may change with temperature, the consistent observation that T_m increased with urate concentration suggests that protein in which only one ligand binding is occupied is less stable than protein with both sites occupied, perhaps because ligand bound to only one site imposes an asymmetry. This interpretation is consistent with the Koshland–Némethy–Filmer (KNF) model of cooperativity and suggests that changes in interaction between subunits are responsible for both the reduced stability of the singly liganded

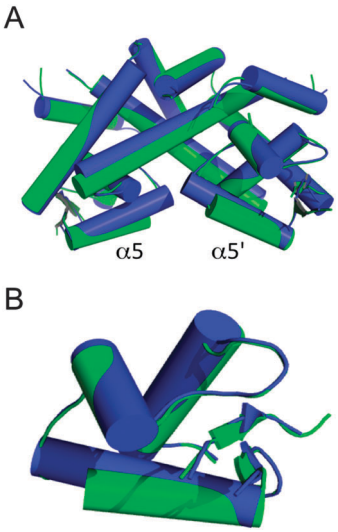

Fig. 6 Structural comparison between HucR-WT and HucR-E48Q. (A) Superimposition of HucR-WT (blue) and HucR-E48Q (green). The long, central α2 helices form the scaffold of the dimer interface and residues H51 and H51′ are located where α2 helices intersect, as shown in Fig. 1. (B) The DNA binding domain showing significant conformational change in the DNA binding helix (α5).

state and for the conformational changes at the second ligand-binding site that lead to reduced affinity (negative cooperativity).

A shift in the melting transition towards higher temperatures on increasing the concentration of urate from 10 μM to 50 μM was also observed for HucR-E48Q and HucR-H51F (Fig. 5B and C). This likewise suggests that occupancy of both ligand-binding sites stabilizes the protein compared to protein in which only one site is filled. Assuming saturation of HucR-E48Q ligand-binding sites with 50 μM urate (for which K_d was ~2 μM), occupancy of both ligand-binding sites in HucR-E48Q led to a modest stabilization (Fig. 5B and Table S2, ESI†). For HucR-H51F, a destabilization was observed on incubation with 50–100 μM urate (Fig. 5C and Table S2, ESI†). This is consistent with fluorescence quenching data, which indicated that substitution of H51 leads to alteration in the dimer interface, affecting communication of ligand occupancy between sites. That HucR-E48Q was marginally stabilized on urate binding to both sites, combined with its higher affinity for urate, may be due to additional flexibility in the dimer interface as a result of removing contacts between H51 and E48 and a correspondingly lower energetic penalty of conformational changes associated with ligand binding.

Changes in the dimer interface propagate to the DNA-binding lobes

The HucR-E48Q crystal structure was determined to 2.05 Å resolution and refined to an *R* factor of 0.256 (Table S3, ESI†). The superimposition of HucR-E48Q on HucR-WT yields an RMSD of 0.26 Å, indicating that the overall topology is unchanged by the mutation. Particularly, the "upper" half of the HucR-E48Q structure was similar to HucR-WT (Fig. 6). This region includes the ligand-binding pocket located between the DNA-binding region and α2, which is consistent with urate binding by HucR-E48Q. However, a small shift in Cα was noticed, starting from the dimerization helix (α2) and propagating towards the DNA binding lobe. In HucR-E48, the distance between H51 and H51′ was 3.44 Å as compared to 3.6 Å in HucR-WT, perhaps due to absence of a salt bridge between H51 and E48. This leads to α2 helices moving towards each other. No significant deformation was observed in the dimerization helices (α2), indicating that the movement is due to a rigid body motion. As a consequence, significant conformational differences were observed in the DNA-binding lobes. The 3-residue 3_{10} helix present at the N-terminus of the recognition helices (α5/α5′) of HucR-WT was better modeled as a loop in HucR-E48Q, resulting in an overall shortening of the helix. This could result in loss of specificity for DNA as observed in the EMSA assay. By comparison, the structure of the MarR homolog OhrR in complex with DNA shows H-bond or van der Waals contacts between DNA bases and a Ser and a Thr, respectively, at the N-termini of DNA recognition helices, indicating that contacts involving the N-termini of recognition helices may contribute to specificity.[35] Furthermore, the short β-strands that constitute the "wing" that follows the helix-turn-helix motif were more pronounced in HucR-E48Q. Since residues in the wing (corresponding to R118 in HucR) are important for affinity and not specificity,[30] this may contribute to high affinity binding by HucR-E48Q. We were unable to obtain HucR-H51F crystals, despite multiple attempts.

Conclusions

For several MarR homologs, it has been shown that ligand binds in a cleft between the dimer interface and the helix-turn-helix DNA-binding motif. Thus, ligand-binding may be directly sensed by the DNA-binding motif. The location of this shared ligand-binding pocket further suggests a mechanism by which occupancy of one site is sensed at the other, as ligand may interact directly with the long helices that form the scaffold of the dimer interface (α2 in HucR). Our data suggest that occupancy of one ligand-binding site reduces protein stability compared to protein in which both sites are occupied. Combined with the observed negative cooperativity of binding to urate, we speculate that occupancy of a single site may suffice for attenuation of DNA binding, thereby ensuring a more sensitive response to ligand and fine-tuned transcriptional control.

HucR exists in a molten globule state at pH 5.0, suggesting that protonation prevents the protein from acquiring a stable 3D structure (Fig. S7, ESI†). Binding of DNA appears to restore a close-packed ordered form (albeit with limited thermal stability). In contrast, HucR-H51F adopts a native folded conformation at pH 5.0. Deprotonation efficiently restores the ordered packing of HucR; this indicates that stacked histidines constitute a reversible molecular switch that controls a large conformational change. Large-scale conformational transitions constitute one mechanism by which protein function may be regulated, and the design of such conformational switches has met with notable successes. Our data suggest that HucR contains such a built-in

molecular switch that may be utilized in synthetic network devices designed to respond to changes in pH.

Experimental

Preparation of HucR mutant proteins

Residues in the HucR dimer interface were mutated by whole-plasmid PCR using as template the recombinant plasmid, which contains the gene encoding *D. radiodurans* HucR without any tags.[9] HucR-E48Q was purified according to the previously reported protocol for HucR,[9] whereas the HucR-H51F purification method was modified. For details, see Supplemental experimental procedures (ESI†). The purity of protein was verified by SDS-PAGE, and the concentration determined by Micro BCA Protein Assay Kit (Pierce) using bovine serum albumin (BSA) as standard.

Gel filtration chromatography

Gel filtration was performed using a TSK gel G3000SW$_{XL}$ column on an ÄKTA FPLC system (GE Healthcare). The column was equilibrated at 4 °C with 50 mM Tris-HCl pH 7.0 or 50 mM MES pH 5.0, both with 150 mM NaCl. A flow rate of 0.8 ml min^{-1} was used. A protein marker (Sigma gel filtration standard) was run on the same column. The markers include β-amylase (200 kDa), alcohol dehydrogenase (150 kDa), bovine serum albumin (66 kDa), carbonic anhydrase (29 kDa), and cytochrome *c* (12.4 kDa). All proteins (including standards) were run on the column at least twice.

Circular dichroism spectroscopy

CD spectroscopy was performed on a Jasco J-815 circular dichroism spectrometer. HucR and mutant proteins (0.2 mg ml^{-1}) were diluted in CD buffer (50 mM sodium phosphate pH 7.0 or 50 mM acetate pH 5.0). Far-UV CD spectra were obtained using a quartz cuvette with 0.1 cm path length at room temperature for pH 7.0 and at 4 °C for pH 5.0. All measurements were collected in triplicate with 1 nm steps over the wavelength range from 250 to 180 nm. The secondary structure composition was predicted from the spectrum by the CDSSTR algorithm with protein reference set 7 from DichroWeb.[36,37] The goodness of fit was determined from the NRMSD value, which was in the range of 0.001–0.016.

For thermal denaturation, ellipticity was monitored from 224 to 218 using a 0.1 cm quartz cuvette over the temperature range of 4–70 °C with 1 °C increments. The data were analyzed after correcting for buffer contribution to the signal using the four-parameter sigmoidal equation of Sigma Plot 9.

Thermal shift assay

HucR and mutant proteins were diluted in TSA buffer (50 mM Tris-HCl pH 8.0, HEPES pH 7.0, MES pH 6.0, or Acetate pH 5.0, 100 mM NaCl, and 5× SYPRO Orange dye (Invitrogen)). Fluorescence emission induced by binding of SYPRO orange dye was monitored at a temperature range of 5–90 °C in one-degree increments on an Applied Biosystems 7500 Real Time PCR instrument. The SYBR Green filter was used for fluorescence intensity measurement.[24] Normalized fluorescence is reported. To assess reversibility of pH effects, protein was equilibrated in buffer pH 5.0, following which an aliquot was removed and brought to pH 8.0 by addition of 50 mM Tris-HCl pH 8.0. For protein–DNA interaction, complimentary 40 nt oligonucleotides containing the HucR binding site were purchased. Double stranded DNA was generated by annealing equimolar amounts of complementary oligonucleotides (100 μM) in 10 mM Tris-HCl pH 8.0, 20 mM NaCl, by heating the sample to 90 °C and allowing it to cool to 25 °C. Protein was mixed with DNA in a ratio of 1 : 1.5 and equilibrated for 30 min. For measuring the effect of ligand on protein stability, urate (dissolved in 0.1 M NaOH) was added to protein samples. The resulting data were analyzed using Sigma Plot 9, using the four-parameter sigmoidal equation, which accounts for a single cooperative transition. Multi-phase transitions were analyzed using the same equation applied to data representing individual transitions. The T_m values reported are the average (±SD) of three replicates from three independent experiments.

Electrophoretic mobility shift assay

The DNA binding affinity of HucR and mutant proteins was measured as described.[11] One femtomole of ^{32}P-labeled 77 bp DNA (HucO) comprising the HucR binding site (Fig. S2, ESI†) was incubated with HucR or mutant proteins for 1 h in binding buffer containing 200 mM Tris-HCl pH 8.0 or 200 mM MES pH 5.0 with 8% glycerol, 10 mM EDTA, 0.05% Brij58, 100 μg ml^{-1} bovine serum albumin and 200 mM NaCl. Reaction mixtures were loaded on 8% polyacrylamide gels (39 : 1 (w/w) acrylamide : bisacrylamide, 50 mM Tris pH 8.0 or MES pH 5.0) and electrophoresed in 45 mM Tris-borate, 1 mM EDTA, pH 8.0 or ME buffer (50 mM MES, 1 mM EDTA, pH 5.0) at room temperature for pH 8.0 and at 4 °C for pH 5.0. Gels were dried and exposed to phosphor screens. Equilibrium dissociation constant (K_d) was measured by fitting densitometric data to $f = (n \times [P]/K_d)/(1 + [P]/K_d)$, where f is fraction DNA bound, n is the number of HucR binding sites, and [P] is free protein concentration. K_d is reported as average ± SD from at least three experiments.

Tryptophan fluorescence quenching

A Jasco FP-6300 spectrofluorimeter was used to record emission spectra from 280 nm to 440 nm after exciting samples with an excitation wavelength of 280 nm. HucR or mutant proteins (1.5 μM) were added to FL buffer (40 mM Tris-HCL pH 8.0, 0.2 mM EDTA, 0.1% BRIJ58, 100 mM NaCl, and 10 mM $MgCl_2$) in a 0.5 cm pathlength cuvette. Ligands (dissolved in 0.1 M NaOH) were added to the reaction mixture and incubated for 2 min before fluorescence was measured. Corrections for inner filter effect were performed as described and the percentage quenching was calculated by $Q_{338} = 1 - (F_{corr}\,[X]/F_{corr}\,[0])$, where $F_{corr}\,[X]$ and $F_{corr}\,[0]$ are corrected fluorescence intensities at 338 nm with X μM and 0 μM ligand, respectively.[30] The binding isotherms were generated by fitting data to a nonlinear binding isotherm using the Hill equation, as described.[30]

Protein crystallization and structure determination

Crystallization of HucR-E48Q was performed as described for HucR-WT.[18] The mutant protein crystallized in the same space group as HucR-WT ($P6_1$), with cell dimensions $a = b = 44.93$ and $c = 284.82$ Å. The crystals were flash frozen in liquid nitrogen and diffraction data were collected at the NE-CAT beamline at Advanced Photon Source, Argonne, Illinois.

The structure was solved by molecular replacement using dimeric HucR-WT as a search model (2FBK) with the program PHASER (Phenix). The initial models were built with AutoBuild (Phenix),[38] followed by manual examination and rebuilding in the program COOT.[39] The refinement was performed with programs Phenix.refine, COOT, and REF MAC_5[40] with NCS restraints and TLS refinement. The final refinement was carried out in REF MAC and five cycles of TLS refinement were applied. The final refined structure of HucR-E48Q (2.05 Å) has R_{work} and R_{free} values of 0.216 and 0.256. Data collection and refinement statistics are shown in Table S3 (ESI†). Illustrations were prepared with PyMOL (Schrödinger, LLC, www.pymol.org). Coordinates and structure factors for HucR-E48Q have been deposited in the Protein Data Bank with accession number 5DD8.

Acknowledgements

We thank Yong-Hwan Lee and Svitlana Pakhomova for helpful discussions. Supported by the National Science Foundation (MCB-1515349) and the National Institutes of Health (1R15GM107825-01) to A. G.

Notes and references

1 N. Nandagopal and M. B. Elowitz, *Science*, 2011, **333**, 1244–1248.
2 W. Weber and M. Fussenegger, *Nat. Rev. Genet.*, 2012, **13**, 21–35.
3 H. Ye and M. Fussenegger, *FEBS Lett.*, 2014, **588**, 2537–2544.
4 C. Kemmer, M. Gitzinger, M. Daoud-El Baba, V. Djonov, J. Stelling and M. Fussenegger, *Nat. Biotechnol.*, 2010, **28**, 355–360.
5 C. Geraths, M. Daoud-El Baba, G. Charpin-El Hamri and W. Weber, *J. Controlled Release*, 2013, **171**, 57–62.
6 S. C. Howard, D. P. Jones and C. H. Pui, *N. Engl. J. Med.*, 2011, **364**, 1844–1854.
7 F. P. Wilson and J. S. Berns, *Adv. Chronic Kidney Dis.*, 2014, **21**, 18–26.
8 W. G. Lima, M. E. Martins-Santos and V. E. Chaves, *Biochimie*, 2015, **116**, 17–23.
9 S. P. Wilkinson and A. Grove, *J. Biol. Chem.*, 2004, **279**, 51442–51450.
10 M. N. Alekshun and S. B. Levy, *Cell*, 2007, **128**, 1037–1050.
11 I. C. Perera and A. Grove, *J. Mol. Cell Biol.*, 2010, **2**, 243–254.
12 S. P. Wilkinson and A. Grove, *Curr. Issues Mol. Biol.*, 2006, **8**, 51–62.
13 D. W. Ellison and V. L. Miller, *Curr. Opin. Microbiol.*, 2006, **9**, 153–159.
14 Y. M. Chang, W. Y. Jeng, T. P. Ko, Y. J. Yeh, C. K. Chen and A. H. Wang, *Proc. Natl. Acad. Sci. U. S. A.*, 2010, **107**, 8617–8622.
15 J. R. Davis, B. L. Brown, R. Page and J. K. Sello, *Nucleic Acids Res.*, 2013, **41**, 3888–3900.
16 I. C. Perera, Y. H. Lee, S. P. Wilkinson and A. Grove, *J. Mol. Biol.*, 2009, **390**, 1019–1029.
17 A. Grove, *Curr. Biol.*, 2013, **23**, R142–R143.
18 T. Bordelon, S. P. Wilkinson, A. Grove and M. E. Newcomer, *J. Mol. Biol.*, 2006, **360**, 168–177.
19 B. D. Ratner and S. J. Bryant, *Annu. Rev. Biomed. Eng.*, 2004, **6**, 41–75.
20 D. N. Woolfson, G. J. Bartlett, A. J. Burton, J. W. Heal, A. Niitsu, A. R. Thomson and C. W. Wood, *Curr. Opin. Struct. Biol.*, 2015, **33**, 16–26.
21 E. A. Meyer, R. K. Castellano and F. Diederich, *Angew. Chem., Int. Ed. Engl.*, 2003, **42**, 1210–1250.
22 J. Heyda, P. E. Mason and P. Jungwirth, *J. Phys. Chem. B*, 2010, **114**, 8744–8749.
23 R. Chelli, F. L. Gervasio, P. Procacci and V. Schettino, *J. Am. Chem. Soc.*, 2002, **124**, 6133–6143.
24 F. H. Niesen, H. Berglund and M. Vedadi, *Nat. Protoc.*, 2007, **2**, 2212–2221.
25 G. V. Semisotnov, N. A. Rodionova, O. I. Razgulyaev, V. N. Uversky, A. F. Gripas and R. I. Gilmanshin, *Biopolymers*, 1991, **31**, 119–128.
26 K. P. Tan, T. B. Nguyen, S. Patel, R. Varadarajan and M. S. Madhusudhan, *Nucleic Acids Res.*, 2013, **41**, W314–W321.
27 O. B. Ptitsyn, *Adv. Protein Chem.*, 1995, **47**, 83–229.
28 M. Arai and K. Kuwajima, *Adv. Protein Chem.*, 2000, **53**, 209–282.
29 I. B. Grishina and R. W. Woody, *Faraday Discuss.*, 1994, 245–262.
30 S. P. Wilkinson and A. Grove, *J. Mol. Biol.*, 2005, **350**, 617–630.
31 C. Andresen, S. Jalal, D. Aili, Y. Wang, S. Islam, A. Jarl, B. Liedberg, B. Wretlind, L. G. Martensson and M. Sunnerhagen, *Protein Sci.*, 2010, **19**, 680–692.
32 A. Gupta and A. Grove, *Biochemistry*, 2014, **53**, 4368–4380.
33 P. Cimmperman, L. Baranauskiene, S. Jachimoviciute, J. Jachno, J. Torresan, V. Michailoviene, J. Matuliene, J. Sereikaite, V. Bumelis and D. Matulis, *Biophys. J.*, 2008, **95**, 3222–3231.
34 D. D. Boehr, R. Nussinov and P. E. Wright, *Nat. Chem. Biol.*, 2009, **5**, 789–796.
35 M. Hong, M. Fuangthong, J. D. Helmann and R. G. Brennan, *Mol. Cell*, 2005, **20**, 131–141.
36 L. Whitmore and B. A. Wallace, *Nucleic Acids Res.*, 2004, **32**, W668–W673.
37 L. Whitmore and B. A. Wallace, *Biopolymers*, 2008, **89**, 392–400.

38 P. D. Adams, P. V. Afonine, G. Bunkoczi, V. B. Chen, I. W. Davis, N. Echols, J. J. Headd, L. W. Hung, G. J. Kapral, R. W. Grosse-Kunstleve, A. J. McCoy, N. W. Moriarty, R. Oeffner, R. J. Read, D. C. Richardson, J. S. Richardson, T. C. Terwilliger and P. H. Zwart, *Acta Crystallogr., Sect. D: Biol. Crystallogr.*, 2010, **66**, 213–221.
39 P. Emsley, B. Lohkamp, W. G. Scott and K. Cowtan, *Acta Crystallogr., Sect. D: Biol. Crystallogr.*, 2010, **66**, 486–501.
40 G. N. Murshudov, P. Skubak, A. A. Lebedev, N. S. Pannu, R. A. Steiner, R. A. Nicholls, M. D. Winn, F. Long and A. A. Vagin, *Acta Crystallogr., Sect. D: Biol. Crystallogr.*, 2011, **67**, 355–367.

